Nanoscale Advances

ROYAL SOCIETY OF CHEMISTRY

PAPER

View Article Online
View Journal | View Issue

Cite this: *Nanoscale Adv.*, 2021, **3**, 1954

Synthesis of naked vanadium pentoxide nanoparticles

Patrick Taylor,*[a] Matthew Kusper,*[a] Tina Hesabizadeh,[a] Luke D. Geoffrion,[a] Fumiya Watanabe,[b] Etienne Herth[c] and Grégory Guisbiers[a]

Received 11th January 2021
Accepted 16th February 2021

DOI: 10.1039/d1na00029b

rsc.li/nanoscale-advances

Vanadium pentoxide is the most important vanadium compound by being the precursor to most vanadium alloys. It also plays an essential role in the production of sulfuric acid as well as in metal-ion batteries and supercapacitors. In this paper, pulsed laser ablation in liquids is used to synthesize "naked" vanadium pentoxide nanostructures. The resulting particles take up "nearly-spherical" and "flower-like" morphologies, composed of α-V_2O_5 and β-V_2O_5 crystalline phases. Even "naked", the nanostructures are stable in time with a zeta potential of −51 ± 7 mV. In order to maximize the production of vanadium pentoxide nanostructure, the optimal repetition rate was determined to be @ ∼6600 Hz when irradiating a pure vanadium target in DI-water. This corresponds to a cavitation bubble lifetime of around ∼0.15 ms. At that repetition rate, the production reached ∼10 ppm per minute of irradiation. Finally, from the characterization of the α-V_2O_5 and β-V_2O_5 nanostructures, the surface energy of each phase has been carefully determined at 0.308 and 1.483 J cm^{-2}, respectively. Consequently, the β-phase was found to display a surface energy very close to platinum. The exciton Bohr radius has been determined at 3.5 ± 0.7 nm and 2.0 ± 0.6 nm for α-V_2O_5 and β-V_2O_5 phases, respectively.

1 Introduction

Vanadium (V) is a transition metal discovered in 1801 by the mineralogist Andrés Manuel del Río in Mexico.[1] It is the 6th most abundant transition metal on Earth, the 21st most abundant chemical element in the Earth's crust and the 2nd most abundant chemical element in seawater.[2–5] The world top 3 producers and reserve holders are China, South Africa and Russia.[2,6] Domestically, the United States has reserves estimated to 45 000 tons. Utah is the primary producer with its White Mesa mill located South East of the state on the Colorado Plateau; while Arkansas, Delaware, Ohio, Pennsylvania and Texas are secondary producers.[6] The importance of vanadium in chemistry is due to its wide range of oxidation states. Indeed, vanadium is often found in oxides with the following oxidation states +5 (V_2O_5), +4 (VO_2), +3 (V_2O_3) and even +2 (VO). The most important oxide is vanadium pentoxide (V_2O_5, also known as *vanadia*) which is used as a catalyst for the production of sulfuric acid.[5] Platinum used to be the catalyst for this chemical reaction; however, as platinum reacts with arsenic impurities possibly present in the sulphur feedstock, V_2O_5 is now preferred. V_2O_5 is also suitable in electrochemical applications.[7,8] Indeed, V_2O_5 has been extensively studied as electrode materials in lithium-ion batteries (LIBs),[9–11] in aluminum-ion batteries (AIBs),[12] zinc-ion batteries (ZIBs)[13,14] and in supercapacitors[15,16] due to its unique crystalline structure. It is also used as a nano-powder in latent finger print detection (LFPD).[17] Furthermore, the surface of V_2O_5 undergoes an insulator–metal transition (IMT) around ∼350–550 K (ref. 18 and 19) and this property has been successfully used to build nitrogen dioxide sensors.[20] Additionally, V_2O_5 is also used in photo-detectors.[21]

Vanadium pentoxide has three polymorphs, α-V_2O_5 (orthorhombic), β-V_2O_5 (monoclinic or tetragonal) and δ-V_2O_5 (orthorhombic).[22] The α-V_2O_5 phase is the most stable phase and the other two phases can be obtained under high pressure and high temperature.

V_2O_5 nanostructures (NSs) has been produced by wet-chemistry[23] and pulsed laser deposition.[24] But only a small number of groups have investigated the synthesis of vanadium oxide NSs by Pulsed Laser Ablation in Liquids (PLAL).[25,26] PLAL synthesis has several advantages compared to wet-chemistry, the main one is that the surface of the synthesized nanoparticles is totally free of any contaminants *i.e.* left-over from chemical reactions or surfactants. This surface purity is really important for nanoparticles used as catalysts or bio-medical agents. In this work, we present a new synthesis protocol to produce "naked" (*i.e.* free of any contaminants) V_2O_5 NSs. Those V_2O_5 NSs are great candidates to be used in catalytic and biomedical applications. The synthesis and characterization are

[a]*Department of Physics and Astronomy, University of Arkansas at Little Rock, 2801 South University Avenue, Little Rock, AR 72204, USA. E-mail: gxguisbiers@ualr.edu*
[b]*Center for Integrative Nanotechnology Sciences, University of Arkansas at Little Rock, 2801 South University Avenue, Little Rock, AR 72204, USA*
[c]*Centre de Nanosciences et de Nanotechnologies, CNRS UMR 9001, Univ. Paris-Sud, Université Paris-Saclay, 91120, Palaiseau, France*

detailed in Sections 2 and 3, respectively. The results and discussion are mentioned in Sections 4 and 5, respectively. Finally, the conclusions are described in Section 6.

2 Materials and methods

A Q-switched Nd:YAG laser from Electro Scientific Industries operating @ 1064 nm was used to irradiate a vanadium target. Bulk vanadium flakes (99.5% from Johnson Matthey) were used as the target in this experiment. The dimensions of the flakes are ~2 mm by ~2 mm. The flakes were rinsed in DI water and then immersed in 5 ml of DI water, contained in a 50 ml rounded single neck glass flask. Consequently, the height of the liquid above the surface of the target was measured to be 8 mm. The pulse repetition rate of the laser was varied from 1 kHz to 10 kHz. Consequently, the pulse duration time varied slightly from 70 ns to 200 ns depending on the repetition rate. The laser shined a pulsed beam with an energy per pulse around 10 mJ per pulse @ 1000 Hz. The beam was deflected by a flat mirror oriented @ 45° angle (with respect to the laser rail) in order to irradiate the target from the top and was then focused by using an 83 mm focal length lens. The beam's spot size on the target was measured by scanning electron microscopy (SEM) to be around ~45 μm. Therefore, the intensity of the laser is determined to be around $\sim 8 \times 10^5$ W cm^{-2}. At 1000 Hz, the fluence is calculated to be $\sim 6 \times 10^{2}$ J cm^{-2}. The target was finally irradiated for 5 min.

The colloidal solutions were characterized by UV-visible spectroscopy (Cary 60 from Agilent), Atomic Emission Spectroscopy (4210 MP-AES from Agilent), Raman Spectroscopy (EZRaman-N from Enwave Optronics, Inc.), X-ray diffraction (Bruker D8-Discover Diffractometer), X-ray Photoelectron Spectroscopy (K-Alpha XPS from Thermo Scientific), Dynamic Light Scattering (NanoBrook 90Plus Zeta from Brookhaven Instruments Corporation), Scanning Electron Microscopy (JEOL JSM – 7000F SEM, equipped with a field emission gun and operating at 30 kV) and Transmission Electron Microscope (JEOL-JEM-2100F TEM operating at 80 kV).

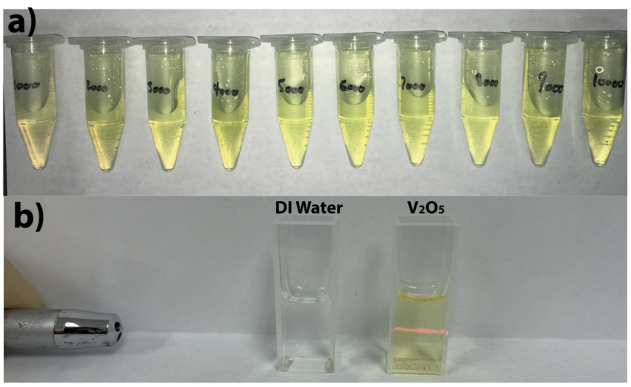

Fig. 1 (a) Photo of the colloidal solutions synthesized at different repetition rate from 1000 Hz to 10 000 Hz. (b) Tyndall effect observed on one of the V_2O_5 colloidal solution.

To perform Raman, XRD and SEM analysis, a droplet of the colloidal solution was deposited onto a silicon wafer and dried in an environmentally controlled glove box. The TEM analysis was performed using a copper TEM grid. X-ray Photoelectron Spectroscopy (XPS) has been performed by using the following etching condition, 200 eV for 20 seconds. The XPS spectra was analyzed with the fitting software, called Avantage.

3 Results

From the direct observation of all the colloidal solutions, it is observed that they all exhibit a yellow color (Fig. 2a). The vanadium oxide stoichiometry of the NSs can be guessed directly from the color of the colloidal solution.[9] Indeed, vanadium exhibits four common oxidation states +5, +4, +3, and +2, each of which can be distinguished by its color, yellow for +5, blue for +4, green for +3 and violet for +2.[9] As the color of the colloidal solutions obtained by pulsed laser ablation is yellow, it

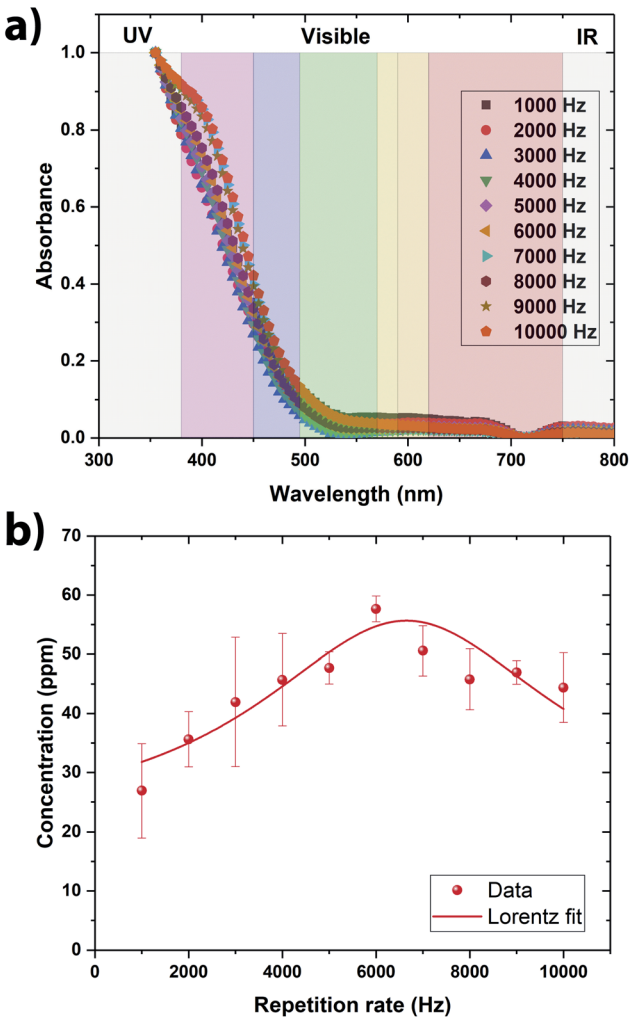

Fig. 2 (a) UV-visible spectra of all the samples. (b) Concentration of vanadium *versus* the laser repetition rate. The vanadium concentration was measured by Atomic Emission Spectroscopy (4210 MP-AES from Agilent). The maximum is reached at ~6600 Hz. The irradiation time was set to 5 min for all samples.

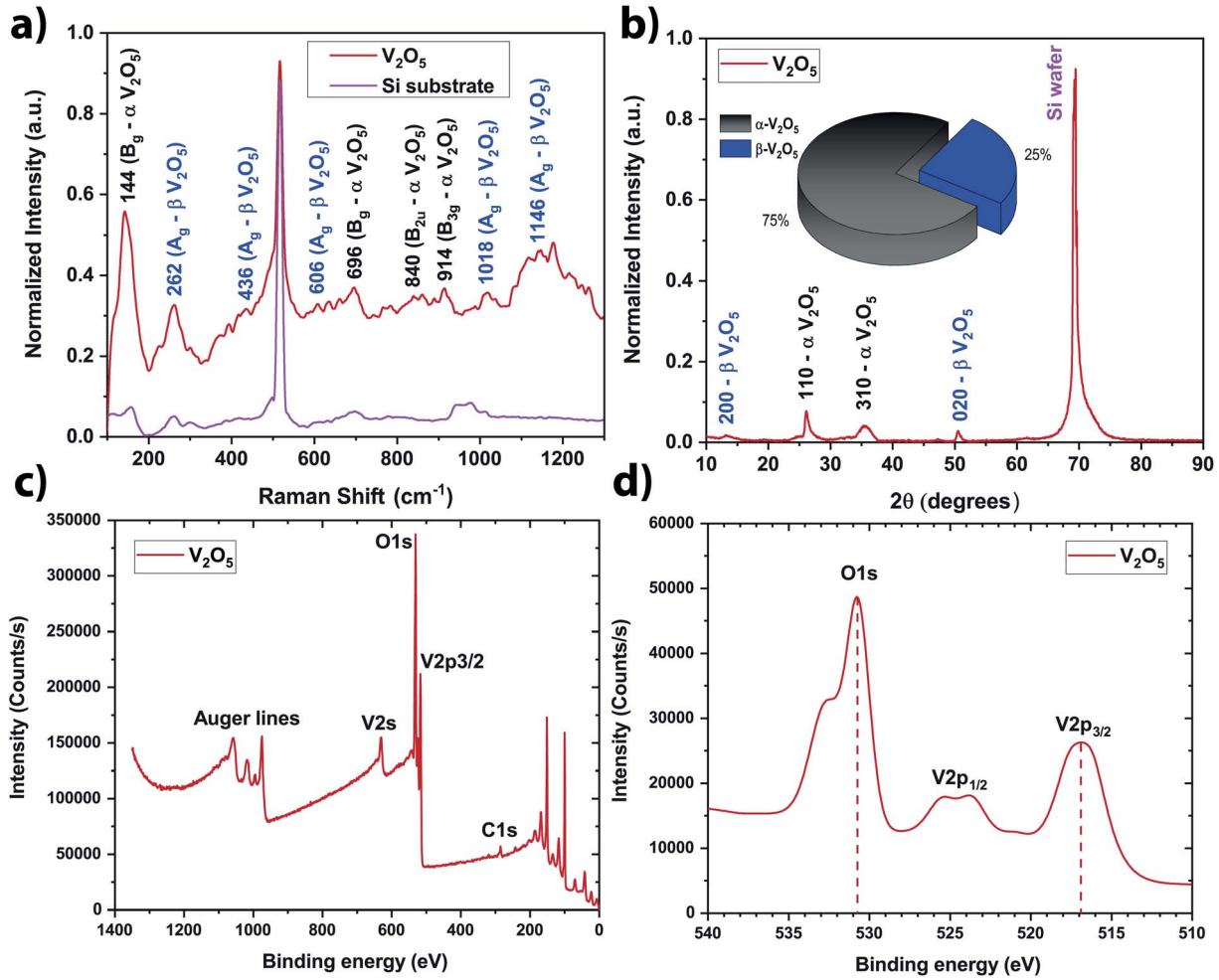

Fig. 3 (a) Raman spectra of the NSs synthesized @ 6600 Hz and the silicon substrate. The identified modes of vibration indicates the formation of V_2O_5 structure. The laser of the Raman spectrometer was 532 nm and its power was 0.5 mW. (b) XRD spectrum of the NSs synthesized @ 6600 Hz. Inset: crystallinity repartition between α-V_2O_5 and β-V_2O_5 (c) wide and (d) narrow XPS spectra of the NSs synthesized @ 6600 Hz.

is evident that V_2O_5 has been produced (Fig. 1a). By shining a pointer laser beam through each sample, the Tyndall effect was observed as illustrated in Fig. 1b. Indeed, the Tyndall effect is the scattering of light as a laser beam passes through a colloidal solution. The presence of particles scatter and reflect the laser light, making the laser beam visible.[27,28] The high oxidation state of vanadium make the NSs absorbing mainly in the violet region, consequently displaying the complementary color in the yellow region (Fig. 2a). From the UV-visible spectroscopy analysis, it seems that the colloidal solutions synthesized at 6000 Hz and 7000 Hz were the ones that absorbs the most in the UV-visible region meaning consequently that they contain the largest amount of NSs (Fig. 2a).

In order to be quantitative, the vanadium concentration contained in each colloidal solution was determined by Atomic Emission Spectroscopy (AES). The data were plotted in Fig. 2b. By fitting the data, the optimal repetition rate producing the highest vanadium concentration was determined to be around 6652 Hz ± 290 Hz. By taking the reciprocal value of this repetition rate, the cavitation bubble lifetime can be estimated around 0.15 ms ± 0.01 ms. This value is similar to the one obtained when irradiating metallic target in deionized water.[29–32] Hitting the target at the repetition rate higher than 6652 Hz is not going to produce more nanoparticle in solution because the laser beam is going to hit the cavitation bubble shielding the target from the beam. Therefore, in a static configuration (the laser beam hits always the same spot on the target), the optimal repetition rate was set to 6600 Hz (the smallest repetition rate increment on the ESI laser is 100 Hz). At this repetition rate, the vanadium concentration in the colloidal solution reaches ~55 ppm within 5 min of irradiation (Fig. 2b). As V_2O_5 has several polymorphs, Raman spectroscopy and XRD analysis were performed to determine the exact crystalline structure of V_2O_5 contained in the colloidal solution. The crystalline structure adopted by the NSs produced @ 6600 Hz was the α- and β-V_2O_5 phases as shown by the Raman and XRD spectra (Fig. 3a and b).[7,35] As shown in the inset of Fig. 3b, the quantities of α- and β-phases of V_2O_5 have been evaluated to 75% and 25%, respectively, by calculating the surface area underneath each peak. The β-phase is the first high pressure

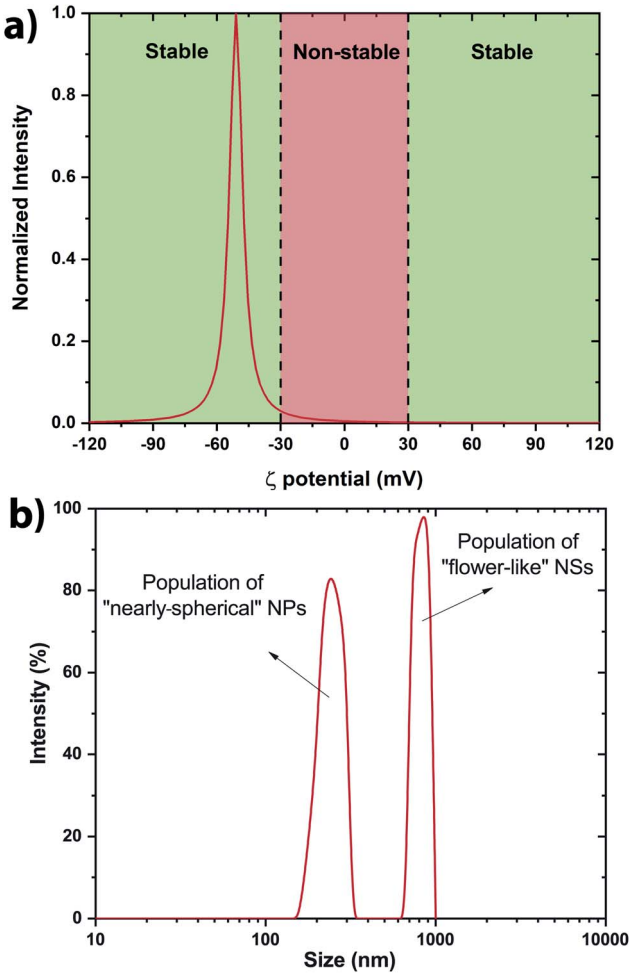

Fig. 4 (a) Zeta potential of V_2O_5 colloidal solution synthesized by PLAL @ 6600 Hz. It has been determined at -51 ± 7 mV. (b) Size distribution measured by dynamic light scattering of V_2O_5 colloidal solution synthesized by PLAL @ 6600 Hz. Two populations have been identified.

phase of V_2O_5 obtained from α-V_2O_5 by the application of isotropic pressure between 4 to 10 GPa at temperatures between room temperature and 1023 K.[36] Based on the synthesis conditions encountered in PLAL, the α-phase seems to be produced during the early stages of bubble expansion while the β-phase seems to be produced at the end during the cavitation bubble collapse.[37] By using the Scherrer equation,[38] the crystallite size in both phases has been determined around ∼13 nm and ∼6 nm for the α- and β-V_2O_5 phases. Furthermore, the XPS spectra are shown on Fig. 3c and d. The C 1s, O 1s, and V 2p core levels were measured. The peak located at ∼517 eV corresponds to the V^{5+} oxidation state meaning that V_2O_5 is found at the surface of the NSs.[39–41]

The stability of the NSs present within the colloidal solution has been determined by measuring the ζ potential.[42,43] It has been measured at -51 ± 7 mV indicating a stable colloidal solution (Fig. 4a). Indeed, solutions with ζ potential smaller than −30 mV or larger than +30 mV are considered as stable. The negative sign of the ζ potential means that the net charge of the scattering NS is negative. This prevents the structure from further reacting within its own environment. A rough estimation of the size distribution has been performed by Dynamic Light Scattering (DLS) revealing two main populations within the colloidal solutions (Fig. 4b). Scanning electron microscopy (SEM) was also performed to determine accurately the morphology of the V_2O_5 NSs.

From Fig. 5, it is clear that two main populations were produced. One population is made of "nearly-spherical" NPs with sizes below 100 nm. The other population is made of "flower-like" type of NSs with an overall size of almost a micron. The flower like structure seems to be linked to the natural tendency of V_2O_5 to grow as a monolayer.[44] Furthermore, a closer look at the NSs by Transmission Electron Microscopy (TEM) revealed that the "nearly-spherical" NPs were adopting an α-phase V_2O_5 while the "flower-like" type NSs were adopting the β-phase V_2O_5 (Fig. 6). Finally, the energy bandgap of both types of NSs was determined by using the Tauc plot (Fig. 7). The Tauc plot is achieved by plotting $(\alpha h\nu)^{1/r}$ *versus* the energy of light using 1/2 as numerical value for the parameter r. The value of r denotes the nature of the transition: $r = 1/2$ for a direct transition while $r = 2$ for an indirect transition. By extrapolating the linear regime of the Tauc plot to the abscissa yields to the energy bandgap.[45,46] From Fig. 7, two energies bandgap were determined at 2.50 eV and 3.65 eV, both corresponding to a direct transition. At the bulk scale, the energies bandgap of α- and β-V_2O_5 have been determined at 2.30 and 3.45 eV, respectively.[47,48] Therefore, it is normal to measure a slightly larger value for each energy bandgap due size effects affecting material properties at the nanoscale.[49,50]

4 Discussion

The first paper reporting the synthesis of vanadium pentoxide nanoparticles by PLAL was published by Celestino-Santos *et al.*[33] in 2011. The particles were distributed into two populations, one around ∼10 nm and another one around ∼60 nm. The nanoparticles are a mixture of amorphous and β-V_2O_5 phases. The second paper from the same group was published in 2012 by Bezerra *et al.*[34] who also reported the synthesis of β-V_2O_5 NPs. The size of nanoparticles ranges from a couple of nm to more than 100 nm.

In this paper, α- and β-V_2O_5 NSs were obtained by irradiating, at high repetition rate *i.e.* in the kHz regime, a target made of vanadium flakes immerged into de-ionized (DI) water. A new morphology was synthesized beside the "nearly spherical" NPs, and it looks like a "flower-like" NSs. All the groups used either distilled or de-ionized water as solvent. All the groups used a nanosecond laser meaning that the pulse duration is in the nanosecond regime. A table summarizing the synthesis conditions of all the groups is shown in Table 1.

To be complete, there is a paper published in 2019 by Val'yano *et al.*[51] who reported the synthesis of $V_{16}O_3$ by PLAL. The average nanoparticle size was around ∼45 nm. Most of the synthesized nanoparticles were amorphous. The target was rotating at 2 rpm so the irradiation spot was circularly displaced on the target surface. Therefore, the key parameters to produce

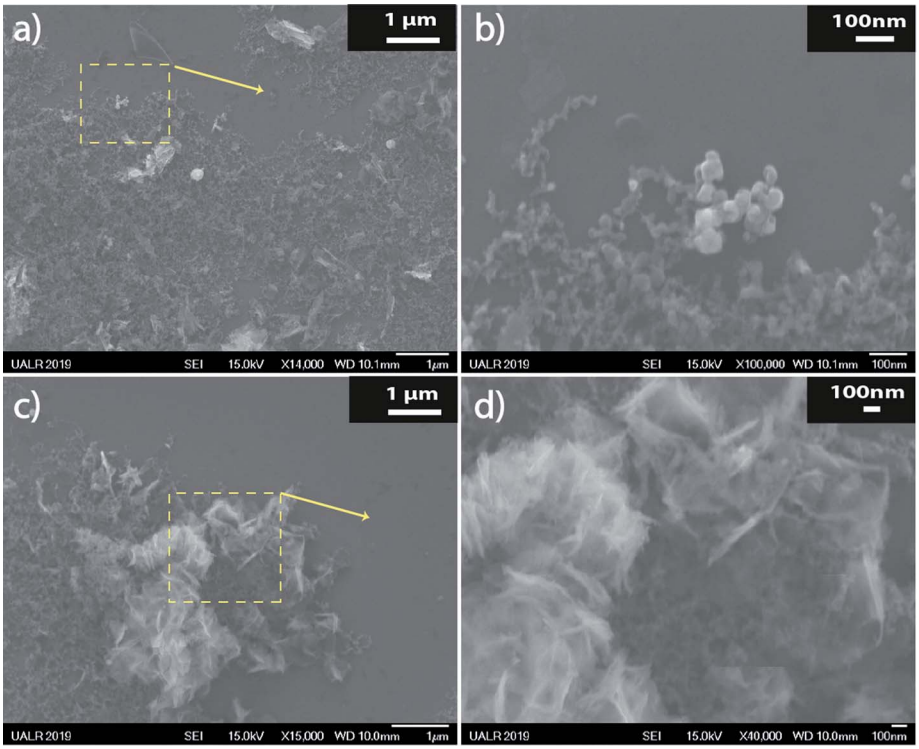

Fig. 5 (a)–(d) SEM images of the NSs synthesized @ 6600 Hz (JEOL JSM – 7000F SEM). Various populations of V_2O_5 NSs are observed but two main populations can be distinguish such as nearly-spherical NPs (a and b) and such as some flower-type of nanostructure (c and d). Images (b) and (d) have been taken within the red square indicated in images (a) and (c), respectively.

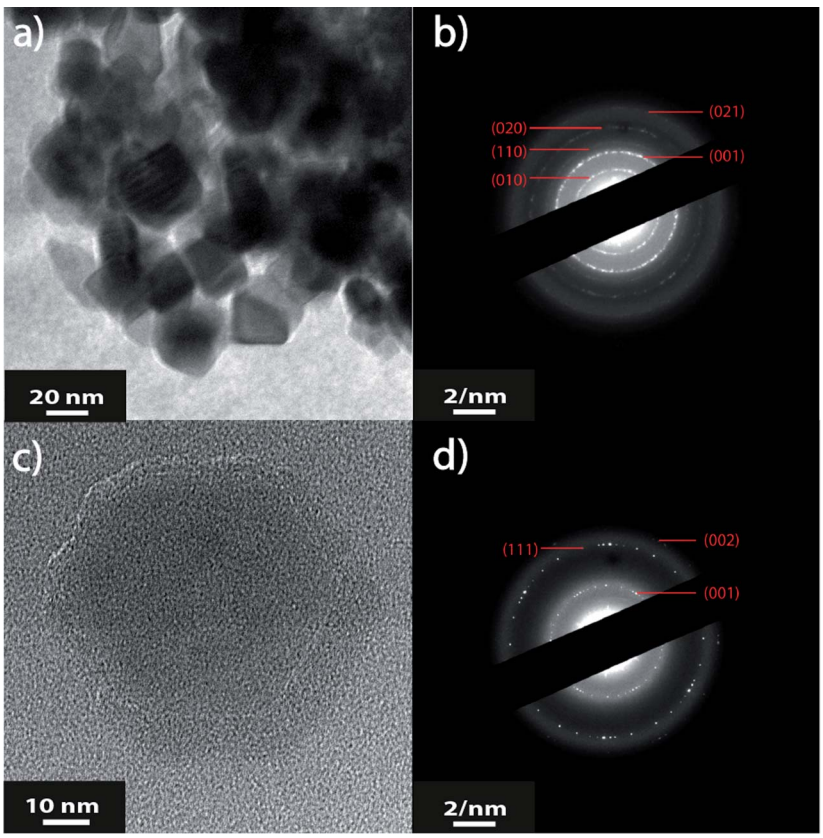

Fig. 6 (a) TEM image of the nearly spherical V_2O_5 NPs. (b) Diffraction pattern corresponding to (a) and revealing the alpha-phase of V_2O_5. (c) TEM image of the "flower-like" type of V_2O_5 NSs. (d) Diffraction pattern corresponding to (c) and revealing the β-phase of V_2O_5.

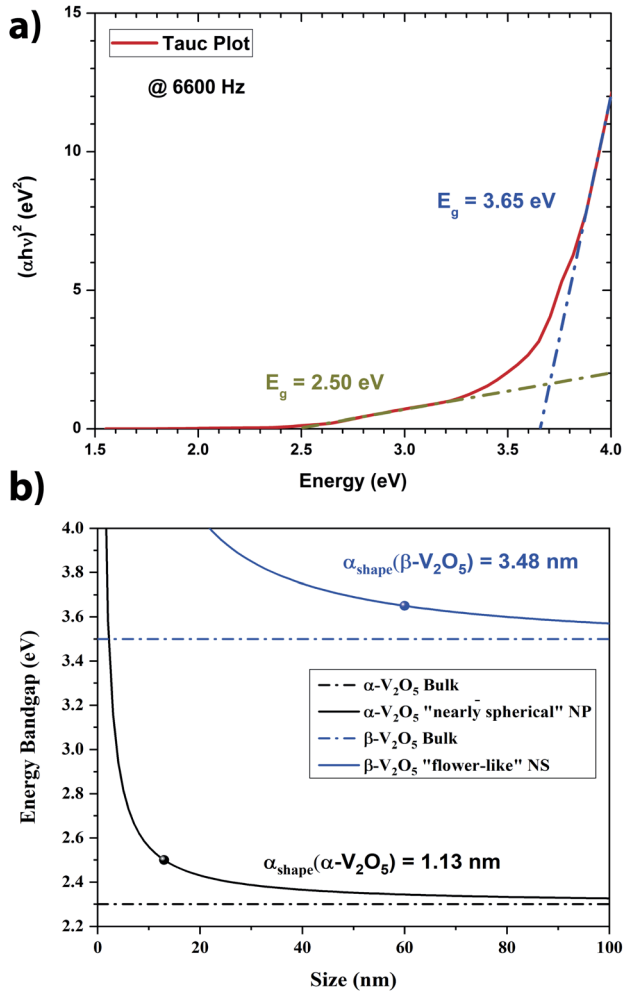

Fig. 7 (a) Tauc plot of the V_2O_5 NSs synthesized @ 6600 Hz by PLAL. Two energy bandgaps have been identified at 2.50 eV and 3.65 eV. (b) Size effect on the energy bandgap of V_2O_5 calculated by nano-thermodynamics.

Table 1 List of all vanadium pentoxide NPs and NSs synthesized by PLAL

Parameters	Ref. 33	Ref. 34	This work
Type of laser	Nd:YAG	Nd:YAG	Nd:YAG
Wavelength	1064 nm	1064 nm	1064 nm
Repetition rate	0.3 kHz	1 kHz	1–10 kHz
Pulse duration	150 ns	200 ns	75–200 ns
Fluence	~80 J cm^{-2}	~80 J cm^{-2}	76–764 J cm^{-2}
Irradiation time	10 min	265 min	5 min
Solvent	Distilled water	Distilled water	DI water
Populations	2	1	2
Size	~10 nm & ~60 nm	~6 nm	~13 nm & $x \sim 200$ nm, $y \sim 300$ nm and $z \sim 60$ nm
Crystalline structure	β-V_2O_5	β-V_2O_5	α-V_2O_5; β-V_2O_5
Morphology	Spherical NPs	Spherical NPs	Nearly-spherical NPs; "flower-like NSs"
Potential application	Biomedical sensor	Biomedical sensor	Catalyst

those "flower-like" V_2O_5 NSs seems to be the larger fluence used in this paper and the higher repetition rate.

Theoretically, the size effect on the energy bandgap of V_2O_5 can be predicted by using nano-thermodynamics.[49] According the theory, the energy bandgap of the nanostructure can be expressed as:

$$\frac{E_g(D)}{E_{g,\infty}} = 1 + \frac{\alpha_{shape}}{D} \quad (1)$$

where $E_g(D)$ is the energy bandgap of a V_2O_5 nanostructure having a size D. $E_{g,\infty}$ is the energy bandgap of V_2O_5 at the bulk scale. α_{shape} is the parameter quantifying the size and shape effects on the considered material property. Furthermore, eqn (1) can be rewritten as:

$$\Delta E_g = \frac{\alpha_{shape}}{D} E_{g,\infty} \quad (2)$$

In Fig. 7a, the energy difference, ΔE_g, between the V_2O_5 nanostructure and the bulk has been determined to be 0.2 eV. Therefore, by using the Scherrer equation on the XRD spectra (Fig. 7b) the crystallite size has been determined around 13 nm for the α-V_2O_5 nanostructure. By assuming the crystallite size is the same as the size of the nanostructure, the α_{shape} parameter for an α-V_2O_5 sphere has been determined at 1.13 nm. By assuming a rectangular morphology for the β-V_2O_5 flake having the following dimensions, $x \sim 200$ nm, $y \sim 300$ nm and $z \sim 60$ nm, is estimated to be around 3.48 nm. It is possible to predict the surface energy of α-V_2O_5 and β-V_2O_5 by using the definition of α_{shape}. Indeed, α_{shape} is defined as:

$$\frac{\alpha_{shape}}{D} = \frac{(\gamma_s - \gamma_l)}{\Delta H_{m,\infty}} \frac{A}{V} \quad (3)$$

where γ_s and γ_l are the solid and liquid surface energy of V_2O_5. $\Delta H_{m,\infty}$ is the bulk melting enthalpy of V_2O_5. A/V is the surface to volume ratio of the V_2O_5 nanostructure.

From Table 2, and γ_l are well known experimentally; the surface to volume ratio of the α-V_2O_5 nanostructures is very similar to the one of a sphere ($\sim 6/D$). Therefore, by using $\alpha_{shape} = 1.13$ nm, γ_s is predicted to be around 0.308 J m^{-2}. This value is well within the range of theoretical values, 0.171 and 0.893 J m^{-2}, announced by Kristoffersen *et al.* for α-V_2O_5 (ref. 56) as well as the range of theoretical values 0.047 and 0.550 J m^{-2} reported by Goclon *et al.*[57] By using $\alpha_{shape} = 3.48$ nm for the β-V_2O_5 flake, the γ_s is predicted to be around 1.483 J m^{-2}. It

Table 2 Some material properties of V_2O_5 used to quantify the magnitude of the size effect and the quantum confinement

Material property	α-V_2O_5	β-V_2O_5
$T_{m,\infty}$ (K) (ref. 52)	963	
$\Delta H_{m,\infty}$ (J m^{-3}) (ref. 52 and 53)	1.21×10^9	
γ_l (J m^{-2}) (ref. 54 and 55)	0.080	
γ_s (J m^{-2})	0.308	1.483
$E_{g,\infty}$ (eV) (ref. 47 and 48)	2.30	3.45
a_b (nm)	3.5 ± 0.7	2.0 ± 0.6
α_{shape} (nm)	1.13	3.48

makes sense to get a larger surface energy value for the β-V_2O_5 phase than for the α-V_2O_5 phase, as the α-V_2O_5 is the most thermodynamically stable. Higher surface energies generally correspond to higher surface chemical reactivities; consequently, β-V_2O_5 flake is more catalytically active than α-V_2O_5.[58] Furthermore, the surface energy of β-V_2O_5 flake is very close to the one of Platinum (Pt). Indeed, the surface energy of Pt ranges between 1.464 and 1.935 J m^{-2} depending on its crystalline orientation.[58]

By using the following equation, the atomic Bohr radius of V_2O_5 can also be predicted:[50]

$$\log(a_{B,ex}) = a + b \times \log(E_g) \quad (4)$$

where $a_{B,ex}$ is the exciton Bohr radius expressed in nanometers, E_g is the bulk energy bandgap at 300 K expressed in electron-volts, $a = 1.04434 \pm 0.04976$ and $b = -1.37696 \pm 0.10488$. Consequently, the exciton Bohr radius of α-V_2O_5 and β-V_2O_5 are determined at 3.5 ± 0.7 nm and at 2.0 ± 0.6 nm, respectively. Our values are in agreement with the one reported by Beke ~4.5 nm.[59]

Consequently, in order to obtain quantum nanostructures of V_2O_5 with the PLAL protocol, it is necessary to increase the irradiation time. This can be done by adding a second step irradiation to the current protocol; indeed, the first step is to produce the nanostructures in solution by irradiating the target, while the second step would just irradiate the colloidal solution without the target being present.

5 Conclusion

Vanadium pentoxide nanostructures have been successfully synthesized by PLAL. It is the first time that "naked" V_2O_5 NSs were successfully synthesized by PLAL. The colloidal solution was very stable with time with a zeta potential of -51 ± 7 mV. The lifetime of the cavitation bubble (~0.15 ms) and the optimal repetition rate (~ 6600 Hz) have been determined when the target was kept static with respect to the laser beam. Two main population of NSs have been produced such as "nearly-spherical" NPs and "flower-like" type of NSs. The "nearly-spherical" NPs adopted an α-V_2O_5 phase while the "flower-like" NSs adopted a β-V_2O_5 phase. Furthermore, the surface energies of α- and β-phases have been estimated to 0.308 and 1.483 J m^{-2}, respectively. Additionally, the bandgap energy is determined to be 2.5 and 3.48 eV for the "nearly spherical" NPs and "flower-like" type of NSs, respectively. Finally, a two-steps irradiation protocol is under development to synthesize V_2O_5 quantum structures. Future work will focus on promoting the flower-like nanostructures, as they have similar surface energy to Pt, which makes it a candidate to replace Pt in most chemical reactions. More work is underway to promote the growth of naked "flower-like" nanostructures with a β-V_2O_5 phase in order to design cheaper catalysts and make the synthesis protocol shape-selective.

Conflicts of interest

There are no conflicts to declare.

Acknowledgements

The authors are grateful to the Center for Integrative Nanotechnology Sciences (CINS) of UA Little Rock for sharing their instruments (SEM, TEM and XPS) and partly supported by the french RENATECH network. Finally, P. Taylor and T. Hesabizadeh would also like to thank the McNair Research Program for their financial support.

Notes and references

1 https://www.rsc.org/periodic table/element/23/vanadium.
2 E. F. Baroch, *Vanadium and vanadium alloys*, 2013.
3 D. Rehder, *Met. Ions Life Sci.*, 2013, **13**, 139–169.
4 W. H. Schlesinger, E. M. Klein and A. Vengosh, *Proc. Natl. Acad. Sci. U. S. A.*, 2017, **114**, E11092–E11100.
5 R. R. Langeslay, D. M. Kaphan, C. L. Marshall, P. C. Stair, A. P. Sattelberger and M. Delferro, *Chem. Rev.*, 2019, **119**, 2128–2191.
6 https://pubs.usgs.gov/periodicals/mcs2020/mcs2020 vanadium.pdf.
7 R. Baddour-Hadjean, M. B. Smirnov, K. S. Smirnov, V. Y. Kazimirov, J. M. Gallardo-Amores, U. Amador, M. E. Arroyo-de Dompablo and J. P. Pereira-Ramos, *Inorg. Chem.*, 2012, **51**, 3194–3201.
8 I. Mjejri, M. Gaudon, G. Song, C. Labrugère and A. Rougier, *ACS Appl. Energy Mater.*, 2018, **1**, 2721–2729.
9 Y. Yue and H. Liang, *Adv. Energy Mater.*, 2017, **7**, 1602545.
10 Y. Zhang, Y. Wang, Z. Xiong, Y. Hu, W. Song, Q. Huang, X. Cheng, L.-Q. Chen, C. Sun and H. Gu, *ACS Omega*, 2017, **2**, 793–799.
11 W. Zhong, J. Huang, S. Liang, J. Liu, Y. Li, G. Cai, Y. Jiang and J. Liu, *ACS Energy Lett.*, 2020, **5**, 31–38.
12 A. M. Diem, B. Fenk, J. Bill and Z. Burghard, *Nanomaterials*, 2020, **10**, 247.
13 F. Liu, Z. Chen, G. Fang, Z. Wang, Y. Cai, B. Tang, J. Zhou and S. Liang, *Nano-Micro Lett.*, 2019, **11**, 25.
14 Y. Yang, Y. Tang, G. Fang, L. Shan, J. Guo, W. Zhang, C. Wang, L. Wang, J. Zhou and S. Liang, *Energy Environ. Sci.*, 2018, **11**, 3157–3162.
15 B. Balamuralitharan, I.-H. Cho, J. S. Bak and H. J. Kim, *New J. Chem.*, 2018, **42**, 11862–11868.
16 D. Majumdar, M. Mandal and S. K. Bhattacharya, *ChemElectroChem*, 2019, **6**, 1623–1648.
17 G. R. Navyashree, K. Hareesh, H. Nagabhushana, G. Nagaraju and D. V. Sunitha, *Mater. Res. Express*, 2019, **6**, 084003.
18 M. Kang, I. Kim, S. W. Kim, J. W. Ryu and H. Y. Park, *Appl. Phys. Lett.*, 2011, **98**, 131907.
19 R.-P. Blum, H. Niehus, C. Hucho, R. Fortrie, M. V. Ganduglia-Pirovano, J. Sauer, S. Shaikhutdinov and H.-J. Freund, *Phys. Rev. Lett.*, 2007, **99**, 226103.
20 K. Schneider and W. Maziarz, *Sensors*, 2018, **18**, 4177.
21 W. B. Fu, G. L. Shang, X. X. Gong, L. D. Zhang and G. T. Fei, *J. Mater. Chem. C*, 2017, **5**, 1471–1478.
22 I. P. Zibrov, V. P. Filonenko, S. G. Lyapin and V. A. Sidorov, *High Pressure Res.*, 2013, **33**, 399–408.

23 M. L. T. Ronquillo, P. S. Jacinto, P. Ovalle, L. R. Vázquez, E. C. Martínez, E. Marinero, V. Garibay, *et al.*, *Mater. Sci. Appl.*, 2016, **7**, 484.
24 J. Huotari, J. Lappalainen, J. Puustinen, T. Baur, C. Alépée, T. Haapalainen, S. Komulainen, J. Pylvänäinen and A. L. Spetz, *Procedia Eng.*, 2015, **120**, 1158–1161.
25 V. Amendola and M. Meneghetti, *Phys. Chem. Chem. Phys.*, 2013, **15**, 3027–3046.
26 D. S. Zhang, B. Goekce and S. Barcikowski, *Chem. Rev.*, 2017, **117**, 3990–4103.
27 E. O. Kraemer and S. T. Dexter, *J. Phys. Chem.*, 1927, **31**, 764–782.
28 S. Yu, Y. Chen and J. Liaw, *2015 International Symposium on Next-Generation Electronics (ISNE)*, 2015, pp. 1–3.
29 M. Kusper and G. Guisbiers, *MRS Adv.*, 2018, **3**, 3899–3903.
30 S. Ibrahimkutty, P. Wagener, A. Menzel, A. Plech and S. Barcikowski, *Appl. Phys. Lett.*, 2012, **101**, 103104.
31 S. I. Kudryashov, A. A. Samokhvalov, A. A. Nastulyavichus, I. N. Saraeva, V. Y. Mikhailovskii, A. A. Ionin and V. P. Veiko, *Materials*, 2019, **12**, 562.
32 L. D. Geoffrion, T. Hesabizadeh, D. Medina-Cruz, M. Kusper, P. Taylor, A. Vernet-Crua, J. Chen, A. Ajo, T. J. Webster and G. Guisbiers, *ACS Omega*, 2020, **5**, 2660–2669.
33 W. Celestino-Santos, A. G. Bezerra, A. B. Cezar, N. Mattoso and W. H. Schreiner, *J. Nanosci. Nanotechnol.*, 2011, **11**, 4702–4707.
34 A. G. Bezerra, A. Barison, V. S. Oliveira, L. Foti, M. A. Krieger, R. Dhalia, I. F. T. Viana and W. H. Schreiner, *J. Nanopart. Res.*, 2012, **14**, 1123.
35 P. Shvets, O. Dikaya, K. Maksimova and A. Goikhman, *J. Raman Spectrosc.*, 2019, 1–19.
36 B. Singh, M. K. Gupta, S. K. Mishra, R. Mittal, P. U. Sastry, S. Rols and S. L. Chaplot, *Phys. Chem. Chem. Phys.*, 2017, **19**, 17967.
37 S. Barcikowski, A. Plech, K. S. Suslick and A. Vogel, *MRS Bull.*, 2019, **44**, 382.
38 J. I. Langford and A. J. C. Wilson, *J. Appl. Crystallogr.*, 1978, **11**, 102–113.
39 https://xpssimplified.com/elements/vanadium.php.
40 M. C. Biesinger, L. W. M. Lau, A. R. Gerson and R. S. C. Smart, *Appl. Surf. Sci.*, 2010, **257**, 887–898.
41 E. Hryha, E. Rutqvist and L. Nyborg, *Surf. Interface Anal.*, 2012, **44**, 1022–1025.
42 S. Bhattacharjee, *J. Controlled Release*, 2016, **235**, 337–351.
43 R. Pecora, *J. Nanopart. Res.*, 2000, **2**, 123–131.
44 K. Schneider, *J. Mater. Sci.: Mater. Electron.*, 2020, **31**, 10478–10488.
45 J. Tauc, R. Grigorovici and A. Vancu, *Phys. Status Solidi*, 1966, **15**, 627–637.
46 P. Makula, M. Pacia and W. Macyk, *J. Phys. Chem. Lett.*, 2018, **9**, 6814–6817.
47 V. V. Porsev, A. V. Bandura and R. A. Evarestov, *Acta Mater.*, 2014, **75**, 246–258.
48 Y. Zhou, Z. Qiu, M. Lü, A. Zhang and Q. Ma, *Mater. Lett.*, 2007, **61**, 4073–4075.
49 G. Guisbiers, *Adv. Phys.: X*, 2019, **4**, 1668299.
50 L. D. Geoffrion and G. Guisbiers, *J. Phys. Chem. Solids*, 2020, **140**, 109320.
51 G. E. Val'yano, T. I. Borodina, V. T. Karpukhin, M. M. Malikov and M. A. Kazaryan, *Bull. Lebedev Phys. Inst.*, 2019, **46**, 273–275.
52 W. Martienssen and H. Warlimont, *Springer handbook of condensed matter and materials data*, 2005.
53 M. J. Ferrante and R. V. Mrazek, *Bureau of Mines Report of Investigations*, 1986, vol. 9039, pp. 1–7.
54 N. Ikemiya, J. Umemoto, S. Hara and K. Ogino, *ISIJ Int.*, 1993, **33**, 156–165.
55 T. Toshihiro, H. Klaus, I. Takamichi and H. Shigeta, *Zeitschrift für metallkunde*, 1996, **87**, 380–389.
56 H. H. Kristoffersen and H. Metiu, *J. Phys. Chem. C*, 2015, **119**, 10500–10506.
57 J. Goclon, R. Grybos, M. Witko and J. Hafner, *J. Phys.: Condens. Matter*, 2009, **21**, 095008.
58 H. Zhuang, A. J. Tkalych and E. A. Carter, *J. Phys. Chem. C*, 2016, **120**, 23698–23706.
59 S. Beke, *Thin Solid Films*, 2011, **519**, 1761–1771.